Single-Molecule Sensing Using Carbon Nanotubes Decorated with Magnetic Clusters

Zeila Zanolli[†,¶,*] and J.-C. Charlier[‡]

[†]Physique Théorique des Matériaux, Université de Liège, B-4000 Sart Tilman, Belgium and [‡]Institute of Condensed Matter and Nanosciences (IMCN), Université catholique de Louvain (UCL), Chemin des étoiles 8, B-1348 Louvain-la-Neuve, Belgium. [¶]Present address: PGI and IAS, Forschungszentrum Jülich, D-52425 Jülich, Germany.

ABSTRACT First-principles and nonequilibrium Green's function techniques are used to investigate magnetism and spin-polarized quantum transport in metallic carbon nanotubes (CNT) decorated with transition metal (Ni_{13}, Pt_{13}) magnetic nanoclusters (NC). For small cluster sizes, the strong CNT−NC interaction induces spin-polarization in the CNT. The adsorption of a benzene molecule is found to drastically modify the CNT−NC magnetization. Such a magnetization change should be large enough to be detected *via* magnetic-AFM or SQUID magnetometry, hence suggesting a novel approach for single-molecule gas detection.

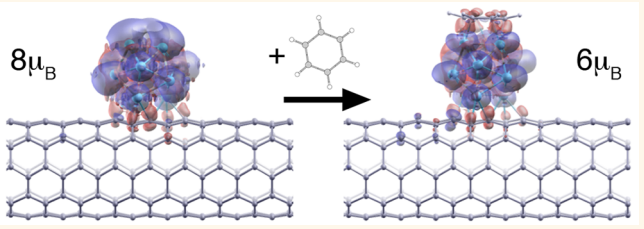

KEYWORDS: spin-polarized quantum transport · nanomagnetism · carbon nanotubes · magnetic nanoclusters · electronic structure · gas sensing

Since their discovery,[1] carbon nanotubes (CNTs) have constantly attracted more interest in the scientific community because of their remarkable electronic and quantum transport properties[2,3] that make them potentially useful for applications in nanoelectronics,[4] spintronics,[5] and gas sensing devices.[6]

Thanks to their high surface-to-volume ratio and being one-dimensional nanosystems, CNTs are considered as exceptional nanodetectors since their properties are extremely sensitive to external perturbations.[6] Hence, CNT-based devices are very promising for ultrasensitive biological[7,8] and chemical[9−15] sensors. However, the sensing ability of devices based on pristine CNTs[9,10] is mostly due to the presence of defects or impurities which perturb the intrinsically inert sp^2 carbon network. To overcome the limitations of pristine CNTs, local functionalization of CNT sidewalls with various chemical groups[11,12] or metal nanoclusters[13−15] has been successfully investigated both experimentally and theoretically. In these CNT-based devices, both the chemical group and the metal NC serve as the sensing unit, as proposed in ref 16. Indeed, gas detection is achieved by macroscopic measurements of the conductivity of modified-CNT mats.[6,13−15]

Moreover, CNTs decorated with transition metal magnetic nanoparticles are also good candidates for spin-dependent transport applications. Indeed, spin-polarized currents can propagate throughout CNTs on extremely long distances (spin diffusion length, ∼1.5 μm[17,18]) thanks to the weak spin−orbit and hyperfine interactions in carbon-based materials, as well as to the large carrier velocity in CNTs. When compared to spin injection by ferromagnetic,[17,19−22] doped magnetic semiconductors,[23] or semimetallic electrodes,[18] CNTs filled with transition metal nanoparticles present the advantage of making an efficient spin injection compatible with low-resistance contacts, as discussed both theoretically[24,25] and experimentally.[26,27]

Here, a new approach to detect individual gas molecules based on local magnetic moment measurements of CNTs decorated with transition metal NCs is proposed. First-principles calculations are used to investigate the perturbation of the electronic, magnetic, and spin-polarized quantum transport properties induced by decorating the external sidewalls of CNTs with Ni and Pt nanoparticles. The presence of these magnetic

* Address correspondence to zeilazanolli@gmail.com.

Received for review September 6, 2012 and accepted November 2, 2012.

Published online November 02, 2012
10.1021/nn304111a

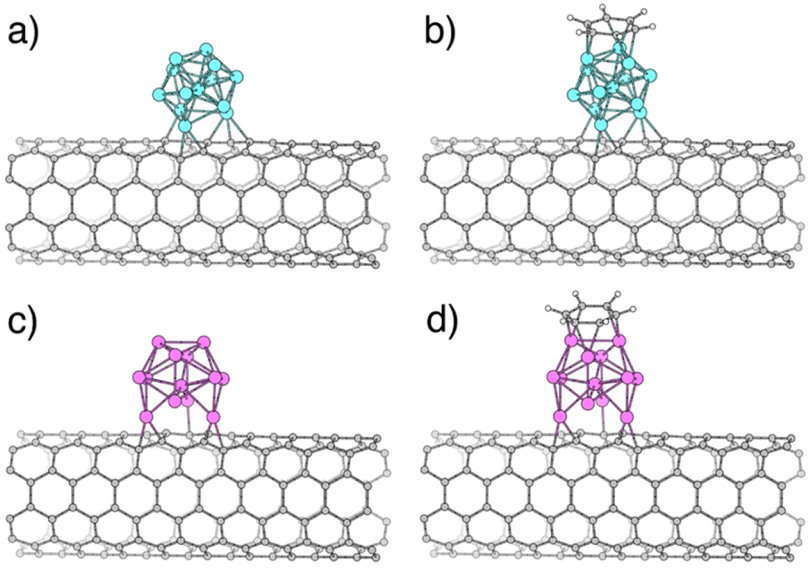

Figure 1. Ball-and-stick schematic models illustrating fully *ab initio* relaxed atomic structures of a (5,5) CNT decorated with a Ni_{13} (a,b) or a Pt_{13} (c,d) nanoparticle before (a,c) and after (b,d) the absorption of a single benzene molecule. Carbon, nickel, platinum, and hydrogen atoms are represented by gray, light blue, pink, and white spheres, respectively.

NCs gives rise to a significant magnetization in the CNT, resulting in a spin-polarized current close to the Fermi energy (E_F). Such induced magnetization is further shown to be drastically affected by the subsequent adsorption of a gas molecule at the NC surface. The computed variations of magnetization in the hybrid CNT−NC system could be detected using either magnetic-AFM measurements at the nanoscale, or a CNT-SQUID device[28] or, even indirectly, exploiting the magneto-Coulomb effect arising by the coupling of the CNT with the magnetic NC,[29] as described in ref 30. Although this new approach implies difficult measurements at the nanoscale, the CNT−NC hybrid systems will exhibit an extraordinary sensitivity to gas molecules with respect to conventional methods based on the macroscopic conductivity measurement performed on CNT mats.

RESULTS AND DISCUSSION

In the present work, a metallic (5,5) singlewall CNT decorated with a Ni_{13} or Pt_{13} nanocluster has been chosen as an ideal model for the CNT−NC system (Figure 1a−c). Indeed, a cluster of 13 atoms corresponds to the minimal size to present a spherical shape (closed atomic shell), and both Ni_{13} and Pt_{13} NCs exhibit extraordinary energetic stability.[31] The icosahedron is known to be the lowest energy structure for Ni_{13}[32] and is also favored for larger cluster sizes. In addition, the magnetic properties of transition metal nanoparticles are strongly size-dependent: the smaller the cluster is, the higher is the magnetic moment per atom. Experimental measurements reported a magnetic moment of ~0.96 μ_B/atom in Ni_{13}[33] and up to ~0.65 μ_B/atom for Pt_{13} in a zeolite.[34] At last, benzene has been selected as the target molecule to detect, since it is an highly toxic gas and just a few studies have reported benzene detection in the ppb range[15] using conventional techniques.

First, the atomic structures of the two isolated Ni_{13} and Pt_{13} NCs, with an icosahedral symmetry, have been fully *ab initio* optimized, finding Ni−Ni and Pt−Pt bond lengths and spin magnetization in excellent agreement with previous *ab initio* calculations: $d_{Ni-Ni} \approx$ 2.25−2.29 Å and $M \approx 8.0\ \mu_B$ for Ni_{13},[35] $d_{Pt-Pt} \approx$ 2.61−2.75 Å and $M \approx 2.0\ \mu_B$ for Pt_{13}.[36]

Second, the equilibrium atomic structures and the electronic properties of the CNT−NC systems (before and after C_6H_6 adsorption) have been computed using a $1 \times 1 \times 9$ periodic supercell (2.2 nm in the *z* direction along the tube axis), for a total of 193 and 205 atoms, respectively. The structural, electronic, and magnetic properties of the CNT−NC systems converge for a real-space grid cutoff of 400 Ry and a $1 \times 1 \times 18$ k-point sampling mesh with a Fermi-Dirac smearing of 10 meV. It is, indeed, necessary to employ a very small electronic temperature since the CNT−NC systems are metallic. The supercell has been optimized along the *z* direction (maximum stress <0.01 eV/Å), while the lateral dimensions are kept fixed ensuring an intertube separation larger than 18 Å. The atomic positions have been relaxed until the maximum force on each atom is less than 0.01 eV/Å. After relaxation, the atomic structure of the Ni_{13} NC keeps its original icosahedral shape, while the Pt_{13} NC is slightly distorted, as depicted in Figure 1 panels a and c, respectively. Both Ni_{13} and Pt_{13} interact strongly with the CNT, as indicated by the large binding energies (E_B) and by the relatively short interdistance (d_{NC}), reported in Table 1. Consequently, this strong interaction between the attached NC and the tube greatly perturbs the pristine CNT band structure

TABLE 1. Computed Bond Lengths, Binding Energies, and Charge Transfer[a]

	Ni_{13}	$Ni_{13}-C_6H_6$	Pt_{13}	$Pt_{13}-C_6H_6$
E_B	−4.514	−4.422	−5.590	−5.748
$E_{B,gas}$		−4.304		−5.918
d_{NC}	1.97	2.22	2.17	2.16
d_{gas}		2.0		2.13
Δq_{NC}	−0.636	−0.662	−0.035	−0.123
Δq_{gas}		0.316		0.148
M	8.0	6.0	4.0	2.6

[a] Computed binding energies (E_B, eV) between the pristine CNT and the two NCs with and without the adsorbed benzene (C_6H_6) molecule, binding energies ($E_{B,gas}$, eV) of the C_6H_6, CNT−NC distance (d_{NC}, Å), NC−C_6H_6 distance (d_{gas}, Å), electronic charge transferred to the NC (Δq_{NC}, $|e|$) and to the benzene molecule (Δq_{gas}, $|e|$). Positive (negative) values of Δq denote an acceptor (donor) character. Net spin polarization (**M**, μ_B) is computed for the whole CNT−NC(+C_6H_6) hybrid system.

(Figure 3a) and, hence, its quantum conductance around E_F, as described later. At last, both NCs are found to exhibit a donor character, with a large electronic charge transfer from the Ni_{13} toward the tube (0.636 e^-) and a smaller one in the case of Pt_{13} (0.035 e^-).

Third, the adsorption of a single benzene molecule on the CNT−NC nanosensor is also investigated theoretically. To model gas adsorption, first-principles conjugate gradient (CG) minimization is performed starting from a benzene ring lying on the top of the NC and parallel to the CNT axis. Indeed, benzene essentially binds thanks to its ring of delocalized π orbitals, that is, with the C_6H_6 ring parallel to the binding surface. The resulting *ab initio* fully relaxed atomic structures are illustrated in Figure 1b−d. Benzene adsorption is found to slightly alter the electronic and structural properties of the CNT−NC hybrid system, as indicated by the almost unchanged CNT−NC distances (d_{NC}) and binding energies (E_B) reported in Table 1. Computed binding energies of the C_6H_6 ($E_{B,gas}$) and NC−C_6H_6 distances (d_{gas}) also suggest that benzene interacts strongly with both Ni and Pt NCs. Consequently, benzene is found to accept a significant fraction of electronic charge from both the CNT−Ni_{13} (0.316 e^-) and the CNT−Pt_{13} (0.148 e^-) hybrid systems. Both the CNT−NC and the NC−C_6H_6 interactions exhibit the conventional features of a chemisorption, that is, high binding energies and relatively short bond lengths. For each geometry, the computed bond lengths, binding energies, and charge transfer are summarized in Table 1.

Magnetic properties and spin-polarized conductances have been calculated using a nonperiodic open-system consisting of a central scattering region and two semi-infinite pristine (5,5) CNTs as left and right electrodes. The scattering region includes the relaxed CNT−NC hybrid system, either with or without adsorbed benzene, embedded between four cells of pristine (5,5) CNT for a total of 17 cells (4.2 nm along the tube axis) and 353 (before) or 365 (after adsorption) atoms. The use of long pristine electrodes is mandatory

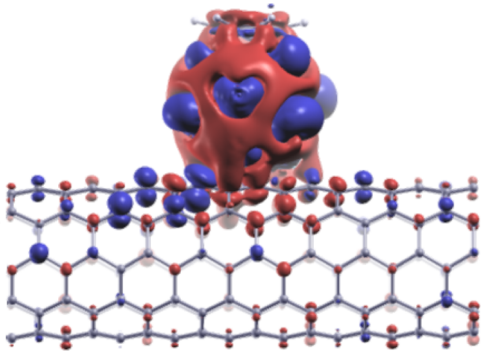

Figure 2. Difference between spin up and spin down densities ($\rho_\uparrow - \rho_\downarrow$) on the CNT-$Ni_{13}$ hybrid system after C_6H_6 adsorption. Blue and red isocurves correspond to positive and negative isodensities of $\rho_\uparrow - \rho_\downarrow$, respectively.

in order to ensure a good screening of the Hartree potential.[12] In addition, the real-space grid cutoff has been raised to 600 Ry in order to guarantee a more accurate description of the electrostatic potential.

The computed magnetization is reported in Table 1 for all the investigated CNT−NC(+C_6H_6) hybrid systems.[37] The net spin polarization of the CNT−Ni_{13} system corresponds exactly to the isolated Ni_{13} NC computed by first-principles ($M \approx 8\,\mu_B$). After benzene adsorption, the electronic charge is redistributed and new bonds are created leading to a decrease of the magnetization to $\sim 6\,\mu_B$. The difference between spin up and spin down densities ($\rho_\uparrow - \rho_\downarrow$) on the CNT-$Ni_{13}$ hybrid system after C_6H_6 adsorption (Figure 2) reveals that the spin magnetization resides mostly on the $Ni_{13}-C_6H_6$ part. However, spin polarization is also induced in the CNT due to the strong coupling between the carbon π states and the Ni *d*-orbitals. An analogous situation occurs for a (5,5) CNT decorated with a Pt_{13} NC during benzene adsorption.

Even though 13 is a magic number for both Ni and Pt NCs, the formation of new bonds in the CNT−NC hybrid system and the resulting charge transfer from the NC to the CNT drives the NC out of this magic number. Benzene adsorption induces a further withdrawal of charge from the NC that, as a consequence, does not go back to the 13-atoms magic number. Hence, the change of magnetic moment due to benzene adsorption is not related to a departure from a magic number state of the NC. Besides, it is worth noticing that the computed change in magnetization after C_6H_6 adsorption depends on the NC size and not only on the adsorbed molecule. Hence, accurate calibration of the experimental setup will be necessary to detect a specific molecule.

After disclosing the structural, electronic, and magnetic properties of two CNT−NC hybrid systems before and after benzene absorption, the spin-polarized quantum electron transport was addressed using the NEGF formalism. In the absence of an external potential and when there is a strong coupling between the scattering

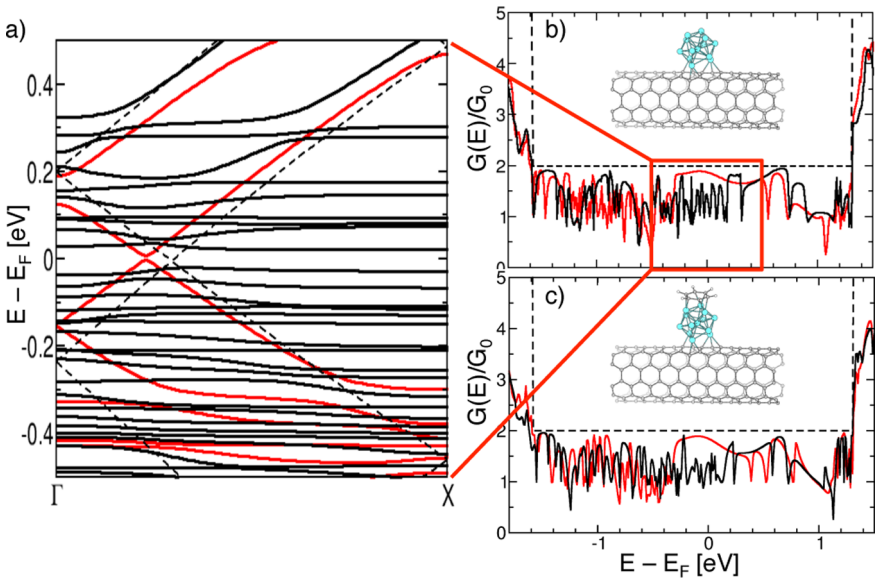

Figure 3. Band structure of the CNT−Ni_{13} hybrid system (a). Conductances in G_0 units of the CNT−Ni_{13} (b) and CNT−Ni_{13}−C_6H_6 (c) hybrid systems. Red and black solid line describe the majority and minority spin channels. Band structure (a) and conductances per spin channel (b, c) of the pristine (5,5) CNT are depicted with dashed lines. The zero energy corresponds to the Fermi level of the pristine (5,5) CNT.

region and the leads, the latter approach is equivalent to the Landauer-Büttiker scheme for equilibrium transport,[38] where the energy dependent electron conductance $G(E)$ and transmission function $T(E)$ satisfy $G(E) = T(E)G_0$, $G_0 = e^2/h$ being the quantum of conductance per spin channel. According to this model, the ballistic conductance of the pristine (5,5) CNT at a given energy is proportional to the number of conducting channels (i.e., the number of bands) at that energy. For instance, in a ideal (5,5) tube, two bands are crossing the Fermi energy (E_F) (Figure 3a, dashed lines) resulting in a conductance of $2G_0$ per spin channel around E_F (Figure 3b,c, dashed lines). The presence of defects, impurities, or, as in the present case, metal decoration and/or gas adsorption perturbs the ideal CNT structure creating scattering centers at certain energy values which cause a decrease of the conductance (from its ideal value) at the corresponding energy.[3] In the present CNT−NC hybrid systems, the very strong interaction between the NC d-orbitals and the carbon π electrons heavily alter the pristine CNT electronic structure, inducing quasi-nondispersive energy bands close to E_F coming from the NC (Figure 3a, solid lines) and distorting the π electron orbitals in the proximity of NC. Consequently, the attached transition metal nanoparticle introduces several scattering centers, thus leading to the many closely spaced dips observed in the conductance curve of Ni-decorated CNTs before (Figure 3b) and after (Figure 3c) benzene adsorption.

Despite the overall strong electron scattering, the conductance of the CNT−Ni_{13} hybrid system is characterized by an energy window of about ∼0.5 eV near E_F where the majority spin current (red curve in Figure 3b) is almost completely transmitted ($G \approx 2G_0$) and the minority spin current (black curve in Figure 3b) is highly backscattered leading to a decrease of the minority conductance to $\sim 1G_0$, that is, to the almost complete suppression of one transmission spin channel. This spin-dependent conducting behavior can be easily explained by analyzing the CNT−Ni_{13} band structure: the majority spin bands (Figure 3a, red curve) differ slightly from the bands of the pristine (5,5) CNT (Figure 3a, dashed curve), while the minority spin bands (Figure 3a, black curve) are highly perturbed due to the CNT−NC interaction. Consequently, CNT−NC hybrid systems could be used to induce spin polarization in unpolarized charge carriers injected *via* low-resistance nonmagnetic electrodes. Near E_F, the spin up electrons will not be affected at all by the presence of the NC, while half of the spin down electrons will be filtered.

Benzene adsorption on the CNT−NC hybrid system does not cause remarkable changes in the transmission function. Despite the fact that C_6H_6 interacts quite strongly with the CNT−NC system, the CNT and NC are already so strongly coupled that the additional interaction with benzene does not affect much the electronic properties of the hybrid system. Consequently, the conductance of the CNT−Ni_{13}−C_6H_6 system (Figure 3c) still presents many closely spaced dips. Owing to the similarity in the quantum conductance before and after C_6H_6 adsorption, it seems difficult to use spin-transport information to predict gas detection. However, the net spin polarization of the CNT−Ni_{13} system is drastically modified by $\sim 2\ \mu_B$ after the adsorption of a single benzene molecule, indicating that a local measurement of the magnetic moment before ($M = 8\ \mu_B$)

and after (M = 6 μ_B) adsorption could, instead, be used to detect tiny quantities of specific gases. Since the nanoscopic size of the NC is crucial to achieve a net spin polarization of the hybrid system, the feasibility of such a detection technique depends on the possibility of decorating CNTs with NCs with diameters in the nanometer range. This nanotechnology challenge has recently been achieved[39] for Ni and Pt nanoclusters of 5.16 and 1.63 nm in diameter, respectively. The local measurement of the magnetic moment of these NCs could then be performed using an AFM with a magnetic tip before and after exposure to gas. Alternatively, a CNT-SQUID device[28] could be used to measure changes of magnetic flux or, at last, an indirect detection of the magnetic moment could be achieved by measuring the changes in physical properties (exchange-field interactions, dipolar couplings, or magneto-Coulomb effects) which are directly induced by the net magnetic moment at the nanoscale.[29,30]

CONCLUSIONS

First-principles and NEGF approaches have been used to investigate hybrid CNT−NC systems (with NC = Ni_{13} and Pt_{13}), before and after C_6H_6 adsorption. The interaction between the CNT π electrons and the NC d orbitals is very strong and deeply affects the pristine CNT structural, electronic, and transport properties. In particular, in the limit of small diameter magnetic NCs, a net spin polarization is induced in the CNT and spin filtering is observed in a small energy window (~0.5 eV) around E_F. Benzene adsorption on the CNT−NC system results in a drastic change of the net magnetic moment. This new magneto-sensing property suggested theoretically, could be exploited as a highly sensitive novel gas detection technique based on the measurement of local magnetic moment in these hybrid CNT−NC systems using various experimental technique such as magnetic AFM or SQUID magnetometer.

METHODS

Ground-state calculations were performed using the SIESTA implementation of the *ab initio* density functional theory (DFT) formalism.[40] Quantum electron transport was modeled within the nonequilibrium Green's function (NEGF) approach using the one-particle DFT Hamiltonian of a SIESTA calculation.[41] Local spin density approximation (LSDA) and norm-conserving pseudopotentials[42] have been employed. A double-ζ (DZ) basis has been chosen for carbon, while a double-ζ polarized (DZP) basis has been optimized for Ni, Pt, and H.[43] Binding energies were computed taking into account the basis set superposition error (BSSE),[44] and atomic charges have been obtained using the Bader decomposition analysis.[45,46] Magnetic moments and spin-polarized quantum transmission curves have been computed using an open-system scheme in order to avoid spurious interactions between magnetic impurities attached to a 1D metallic tube and belonging to nearest-neighbor periodically repeated supercells.[47] Since magnetic interactions are long-ranged, periodic boundary conditions are not suitable to describe the magnetic properties of CNTs[47,48] and graphene[49] containing magnetic impurities. Instead, CNT properties that do not directly involve magnetism (such as structural relaxations, binding energies, local charge transfers, bond lengths) are essentially not affected by long-range interactions and can thus be computed within a periodic boundary condition scheme.

Conflict of Interest: The authors declare no competing financial interest.

Acknowledgment. J.-C.C. acknowledges financial support from the F.R.S.-FNRS of Belgium. This work is directly connected to the Nano2Hybrids project (EC-STREP-033311), to the ARC on "Hybrid metal/organic nanosystems" sponsored by the Communauté Française de Belgique, and to the European Union through the ETSF e-I3 project (Grant No. 211956). Computational resources were provided by the Université catholique de Louvain; all the numerical simulations were performed on the computers of the CISM.

REFERENCES AND NOTES

1. Iijima, S. Helical Microtubules of Graphitic Carbon. *Nature* **1991**, *354*, 56–58.
2. Charlier, J.-C.; Blase, X.; Roche, S. Electronic and Transport Properties of Nanotubes. *Rev. Mod. Phys.* **2007**, *79*, 677–732.
3. Dubois, S. M. M.; Zanolli, Z.; Declerck, X.; Charlier, J. C. Electronic Properties and Quantum Transport in Graphene-Based Nanostructures. *Eur. Phys. J. B* **2009**, *72*, 1–24.
4. Avouris, P.; Chen, Z.; Perebeinos, V. Carbon-Based Electronics. *Nat. Nanotechnol.* **2007**, *2*, 605–615.
5. Kuemmeth, F.; Churchill, H. O. H.; Herring, P. K.; Marcus, C. M. Carbon Nanotubes for Coherent Spintronics. *Mater. Today* **2010**, *13*, 18–26.
6. Goldoni, A.; Petaccia, L.; Lizzit, S.; Larciprete, R. Sensing Gases with Carbon Nanotubes: A Review of the Actual Situation. *J. Phys. Condens. Matter* **2010**, *22*, 013001.
7. Besteman, K.; Lee, J.; Wiertz, F.; Heering, H.; Dekker, C. Enzyme-Coated Carbon Nanotubes as Single-Molecule Biosensors. *Nano Lett.* **2003**, *3*, 727–730.
8. Star, A.; Gabriel, J.; Bradley, K.; Grüner, G. Electronic Detection of Specific Protein Binding Using Nanotube FET Devices. *Nano Lett.* **2003**, *3*, 459–463.
9. Kong, J.; Franklin, N.; Zhou, C.; Chapline, M.; Peng, S.; Cho, K.; Dai, H. Nanotube Molecular Wires as Chemical Sensors. *Science* **2000**, *287*, 622–625.
10. Collins, P.; Bradley, K.; Ishigami, M.; Zettl, A. Extreme Oxygen Sensitivity of Electronic Properties of Carbon Nanotubes. *Science* **2000**, *287*, 1801–1804.
11. Goldsmith, B. R.; Coroneus, J. G.; Kane, A. A.; Weiss, G. A.; Collins, P. G. Monitoring Single-Molecule Reactivity on a Carbon Nanotube. *Nano Lett.* **2008**, *8*, 189–194.
12. Zanolli, Z.; Charlier, J. C. Defective Carbon Nanotubes for Single-Molecule Sensing. *Phys. Rev. B* **2009**, *80*, 155447.
13. Charlier, J.-C.; Arnaud, L.; Avilov, I. V.; Delgado, M.; Demoisson, F.; Espinosa, E. H.; Ewels, C. P.; Felten, A.; Guillot, J.; Ionescu, R.; *et al.* Carbon Nanotubes Randomly Decorated with Gold Clusters: From Nano(2)Hybrid Atomic Structures to Gas Sensing Prototypes. *Nanotechnology* **2009**, *20*, 375501.
14. Zanolli, Z.; Leghrib, R.; Felten, A.; Pireaux, J.-J.; Llobet, E.; Charlier, J.-C. Gas Sensing with Au-Decorated Carbon Nanotubes. *ACS Nano* **2011**, *5*, 4592–4599.
15. Leghrib, R.; Felten, A.; Demoisson, F.; Reniers, F.; Pireaux, J.-J.; Llobet, E. Room-Temperature, Selective Detection of Benzene at Trace Levels Using Plasma-Treated Metal-Decorated Multiwalled Carbon Nanotubes. *Carbon* **2010**, *48*, 3477–3484.
16. Zhao, Q.; Nardelli, M.; Lu, W.; Bernholc, J. Carbon Nanotube−Metal Cluster Composites: A New Road to Chemical Sensors? *Nano Lett.* **2005**, *5*, 847–851.

17. Tsukagoshi, K.; Alphenaar, B.; Ago, H. Coherent Transport of Electron Spin in a Ferromagnetically Contacted Carbon Nanotube. *Nature* **1999**, *401*, 572–574.
18. Hueso, L. E.; Pruneda, J. M.; Ferrari, V.; Burnell, G.; Valdés-Herrera, J. P.; Simons, B. D.; Littlewood, P. B.; Artacho, E.; Fert, A.; Mathur, N. D. Transformation of Spin Information into Large Electrical Signals using Carbon Nanotubes. *Nature* **2007**, *445*, 410–413.
19. Sahoo, S.; Kontos, T.; Furer, J.; Hoffmann, C.; Gräber, M.; Cottet, A.; Schönenberger, C. Electric Field Control of Spin Transport. *Nat. Phys.* **2005**, *1*, 99–102.
20. Kim, J.; So, H.; Kim, J.; Kim, J. Spin-Dependent Transport Properties in a Single-Walled Carbon Nanotube with Mesoscopic Co Contacts. *Phys. Rev. B* **2002**, *66*, 233401.
21. Hoffer, X.; Klinke, C.; Bonard, J.; Gravier, L.; Wegrowe, J. Spin-Dependent Magnetoresistance in Multiwall Carbon Nanotubes. *Europhys. Lett.* **2004**, *67*, 103–109.
22. Tombros, N.; van der Molen, S.; van Wees, B. Separating Spin and Charge Transport In Single-Wall Carbon Nanotubes. *Phys. Rev. B* **2006**, *73*, 233403.
23. Jensen, A.; Hauptmann, J.; Nygå, J.; Lindelof, P. Magnetoresistance in Ferromagnetically Contacted Single-Wall Carbon Nanotubes. *Phys. Rev. B* **2005**, *72*, 035419.
24. Yang, C.; Zhao, J.; Lu, J. Magnetism of Transition-Metal/Carbon-Nanotube Hybrid Structures. *Phys. Rev. Lett.* **2003**, *90*, 257203.
25. Blase, X.; Margine, E. R. Resonant Spin-Filtering in Cobalt Decorated Nanotubes. *Appl. Phys. Lett.* **2009**, *94*, 173103.
26. Soldano, C.; Kar, S.; Talapatra, S.; Nayak, S.; Ajayan, P. M. Detection of Nanoscale Magnetic Activity Using a Single Carbon Nanotube. *Nano Lett.* **2008**, *8*, 4498–4505.
27. Datta, S.; Marty, L.; Cleuziou, J. P.; Tilmaciu, C.; Soula, B.; Flahaut, E.; Wernsdorfer, W. Magneto-Coulomb Effect in Carbon Nanotube Quantum Dots Filled with Magnetic Nanoparticles. *Phys. Rev. Lett.* **2011**, *107*, 186804.
28. Cleuziou, J. P.; Wernsdorfer, W.; Bouchiat, V.; Ondarçuhu, T.; Monthioux, M. Carbon Nanotube Superconducting Quantum Interference Device. *Nat. Nanotechnol.* **2006**, *1*, 53–59.
29. Shimada, H.; Ono, K.; Ootuka, Y. Driving the Single-Electron Device with a Magnetic Field. *J. Appl. Phys.* **2003**, *93*, 8259–8264.
30. Bogani, L.; Wernsdorfer, W. Molecular Spintronics Using Single-Molecule Magnets. *Nat. Mater.* **2008**, *7*, 179–186.
31. Baletto, F.; Ferrando, R. Structural Properties of Nanoclusters: Energetic, Thermodynamic, and Kinetic Effects. *Rev. Mod. Phys* **2005**, *77*, 371–423.
32. Parks, E.; Zhu, L.; Ho, J.; Riley, S. The Structure of Small Nickel Clusters. 1. Ni-3-Ni-15. *J. Chem. Phys.* **1994**, *100*, 7206–7222.
33. Apsel, S.; Emmert, J.; Deng, J.; Bloomfield, L. Surface-Enhanced Magnetism in Nickel Clusters. *Phys. Rev. Lett.* **1996**, *76*, 1441–1444.
34. Liu, X.; Bauer, M.; Bertagnolli, H.; Roduner, E.; van Slageren, J.; Phillipp, F. Structure and Magnetization of Small Monodisperse Platinum Clusters. *Phys. Rev. Lett.* **2006**, *97*, 253401.
35. Calleja, M.; Rey, C.; Alemany, M.; Gallego, L.; Ordejón, P.; Sánchez-Portal, D.; Artacho, E.; Soler, J. Self-Consistent Density-Functional Calculations of the Geometric, Electronic Structures, and Magnetic Moments of Ni−Al Clusters. *Phys. Rev. B* **1999**, *60*, 2020–2024.
36. Liu, X.; Dilger, H.; Eichel, R.; Kunstmann, J.; Roduner, E. A Small Paramagnetic Platinum Cluster in an NaY Zeolite: Characterization and Hydrogen Adsorption and Desorption. *J. Phys. Chem. B* **2006**, *110*, 2013–2023.
37. Since the electric charge is not conserved in the open-system, there is an error in the computed magnetization of ~0.05 e^- for CNT−Ni_{13}, ~0.14 e^- for CNT−Ni_{13}−C_6H_6, ~0.26 e^- for CNT−Pt_{13}, and ~0.42 e^- for CNT−Pt_{13}−C_6H_6.
38. Buttiker, M.; Imry, Y.; Landauer, R.; Pinhas, S. Generalized Many-Channel Conductance Formula with Application to Small Rings. *Phys. Rev. B* **1985**, *31*, 6207–6215.
39. Song, W.; Jeon, C.; Kim, M.; Kwon, Y. T.; Jung, D. S.; Kim, S. Y.; Jung, W. S.; Kim, Y.; Lee, S. Y.; Choi, W. C.; *et al.* The Decoration of Multi-Walled Carbon Nanotubes with Metal Nanoparticles of Uniform Size Using Mev Electron Beam Irradiation. *Carbon* **2011**, *49*, 1692–1698.
40. Soler, J. M.; Artacho, E.; Gale, J. D.; Garcia, A.; Junquera, J.; Ordejón, P.; Sánchez-Portal, D. The SIESTA Method for *ab Initio* Order-N Materials Simulation. *J. Phys.: Condens. Matter* **2002**, *14*, 2745–2779.
41. Rocha, A. R.; Garcia-Suárez, V. M.; Bailey, S.; Lambert, C.; Ferrer, J.; Sanvito, S. Spin and Molecular Electronics in Atomically Generated Orbital Landscapes. *Phys. Rev. B* **2006**, *73*, 085414.
42. Troullier, N.; Martins, J. L. Efficient Pseudopotentials for Plane-Wave Calculations. *Phys. Rev. B* **1991**, *43*, 1993–2006.
43. Junquera, J.; Paz, O.; Sánchez-Portal, D.; Artacho, E. Numerical Atomic Orbitals for Linear-Scaling Calculations. *Phys. Rev. B* **2001**, *64*, 235111.
44. Boys, S.; Bernardi, F. Calculation of Small Molecular Interactions by Differences of Separate Total Energies—Some Procedures with Reduced Errors. *Mol. Phys.* **1970**, *19*, 553–&.
45. Bader, R. F. W. *Atoms in Molecules—A Quantum Theory*; Oxford University Press: Oxford, 1990.
46. Sanville, E.; Kenny, S. D.; Smith, R.; Henkelman, G. Improved Grid-Based Algorithm for Bader Charge Allocation. *J. Comput. Chem.* **2007**, *28*, 899–908.
47. Zanolli, Z.; Charlier, J. C. Spin Transport in Carbon Nanotubes with Magnetic Vacancy-Defects. *Phys. Rev. B* **2010**, *81*, 165406.
48. Kirwan, D. F.; Rocha, C. G.; Costa, A. T.; Ferreira, M. S. Sudden Decay of Indirect Exchange Coupling between Magnetic Atoms on Carbon Nanotubes. *Phys. Rev. B* **2008**, *77*, 085432.
49. Venezuela, P.; Muniz, R. B.; Costa, A. T.; Edwards, D. M.; Power, S. R.; Ferreira, M. S. Emergence of Local Magnetic Moments in Doped Graphene-Related Materials. *Phys. Rev. B* **2009**, *80*, 241413.